

IMPACT TOLERANCE OF DRILLED THICK C/SiC CERAMIC MATRIX COMPOSITES

Antonio Maria Caporale[1], Gerardus Janszen[1],
Abha Sanjay Jambhulkar[1], Mauro Ursic[2], Alessandro Tasca[2], Raffaello Passoni[2] & Alessandro Airoldi[1]

[1] Aerospace Science and Technology Department, Politecnico di Milano, Milano, Italy
[2] Brembo N.V, Curno, BG, Italy

Abstract

Carbon fiber reinforced silicon carbide (C/SiC) Ceramic Matrix Composites (CMCs) are among the most promising materials for high-temperature lightweight aerospace structures. In aeronautical service, low-energy impacts such as tool drops or debris strikes can introduce internal damage with limited external evidence. However, the behavior of CMCs in the presence of Barely Visible Impact Damage (BVID) is still poorly understood, particularly in terms of detectability, residual strength reduction, and fatigue endurance. This work investigates the low-energy impact response, residual flexural strength, fatigue behavior, and constitutive degradation of a 3D reinforced C/SiC composite manufactured by Liquid Silicon Infiltration (LSI), with the objective of defining impact-dependent material allowables for damage-tolerant design. Specimens were extracted from carbon-ceramic brake discs containing cooling holes used as representative open-hole discontinuities. The experimental campaign included impact tests, post-impact flexural characterization, optical microscopy analyses, and cyclic fatigue tests. Damage was observed to initiate on the tensile side, typically from holes located near the specimen edges. Impacts around the BVID threshold produced significant reductions in residual strength, while impact energies above the threshold caused strength reductions exceeding 60%. Nevertheless, fatigue tests showed no crack propagation or stiffness degradation for cyclic loads up to approximately 75% of the residual static strength. A homogenized finite element model was developed to derive effective constitutive laws as a function of the impact energy, enabling a design-oriented characterization of the material degradation. The combined experimental and numerical results provide a framework for the definition of admissible material properties and damage-tolerant methodologies for C/SiC aerospace structures subjected to accidental low-energy impacts.

Keywords: Ceramic Matrix Composites, Impact Engineering, Damage Tolerance, Hot Structures

1. Introduction

Future aerospace systems are increasingly driven by the need for higher efficiency, reduced operational costs, and improved structural capability under extreme thermo-mechanical environments. These requirements demand structural materials capable of combining low density, high thermal stability, and reliable mechanical performance under severe loading conditions. In this context, Ceramic Matrix Composites (CMCs) have emerged as key enabling materials for high-temperature lightweight structures and reusable aerospace systems.

CMCs consist of a ceramic matrix reinforced by continuous fibers, short fibers, or particulate phases. The introduction of reinforcement mitigates the intrinsic brittleness of monolithic ceramics by activating energy-dissipation mechanisms such as crack deflection, crack bridging, interfacial debonding, and fiber pull-out [1]. As a result, CMCs retain the high-temperature capability, oxidation resistance, low creep sensitivity, and thermal stability of ceramics while exhibiting significantly improved fracture toughness and damage tolerance. Depending on the selected matrix and reinforcement systems, these materials can be tailored for demanding structural applications involving combined thermal and mechanical loading.

Among the available CMC families, carbon fiber reinforced silicon carbide (C/SiC) composites are particularly attractive due to their combination of thermal resistance, specific mechanical properties,

and manufacturing versatility [2], [3], [4], [5], [6]. These materials are commonly produced through infiltration-based processes such as Chemical Vapor Infiltration (CVI), Polymer Infiltration and Pyrolysis (PIP), or Liquid Silicon Infiltration (LSI). Such manufacturing routes generate intrinsically heterogeneous microstructures characterized by residual porosity, complex fiber architectures, and residual thermal stresses, leading to nonlinear mechanical responses even under moderate loading conditions [7].

In aeronautical environments, structural components are frequently exposed to accidental low-energy impacts caused by maintenance operations, runway debris, hail, or other foreign objects. Although the associated impact energies are relatively limited, these events may generate localized damage that remains difficult to detect through conventional inspection procedures while still significantly affecting the residual structural capability. The problem is particularly relevant for composite materials, where damage may develop beneath a substantially intact external surface.

For CMCs, the impact damage scenario differs substantially from that of polymer matrix composites. Due to the brittle nature of the ceramic constituents and the heterogeneous architecture of the material, low-energy impacts generally produce localized matrix cracking, fiber/matrix debonding, and confined crack networks [8], [9], [10], [11] rather than large, delaminated regions. In the presence of geometrical discontinuities such as holes, these damage mechanisms become strongly influenced by local stress concentrations, which may promote crack initiation even under relatively limited impact energies.

Within a damage-tolerant design framework, the concept of Barely Visible Impact Damage (BVID) identifies the maximum damage state that can reasonably remain undetected during standard inspection procedures while still requiring the structure to safely sustain the prescribed operational loads until the next inspection interval [12]. For CMC structures, BVID is therefore associated not only with the visual detectability of damage, but also with the onset of structurally significant degradation mechanisms capable of reducing the residual load-bearing capability.

Within this framework, the present work investigates the low-energy impact response, post-impact residual flexural behavior, fatigue performance, and constitutive degradation of a 3D reinforced C/SiC composite manufactured through Liquid Silicon Infiltration (LSI). The objectives of the work are the identification of the BVID threshold, the characterization of the associated damage mechanisms and residual mechanical performance, the evaluation of the fatigue tolerance of impacted specimens, and the development of a numerical approach capable of deriving impact-dependent constitutive properties for damage-tolerant structural design. The specimens were extracted from carbon-ceramic brake discs containing characteristic cooling holes, which also provide representative structural discontinuities for the investigation of open-hole impact-sensitive configurations relevant to lightweight structural applications.

The experimental activity included low-energy impact testing, residual flexural strength characterization, optical microscopy investigations, and fatigue tests under cyclic bending loads representative of service-like conditions. Particular attention was devoted to the identification of the BVID threshold, to the characterization of crack initiation and propagation mechanisms, and to the evaluation of the residual structural capability associated with different impact damage states.

In parallel, a homogenized numerical modeling strategy was developed with the objective of deriving engineering-oriented constitutive laws suitable for impact-tolerant structural design. Rather than reproducing the detailed local damage mechanisms, the numerical activity focused on identifying effective material properties capable of representing the residual flexural response as a function of the impact energy level. The combined experimental and numerical framework therefore provides a basis for the definition of admissible constitutive properties and damage-tolerant methodologies for C/SiC structures subjected to accidental low-energy impacts.

2. Experimental Methods

2.1 Material and specimens

The material under investigation is a C/SiC composite reinforced with a three-dimensional architecture of continuous carbon fibers. A carbon matrix is first produced through a Chemical Vapor Deposition (CVD) process, during which machining operations are performed when required. Subsequently, Liquid Silicon Infiltration (LSI) is carried out to convert the C/C preform into the final ceramic matrix composite material.

Due to the manufacturing route adopted for the brake disc, the orientation of the individual plies follows the circumferential direction of the component. As a consequence, with respect to the extracted

specimens, the reinforcement architecture can be regarded as predominantly longitudinal. From a practical standpoint, reconstructing the exact stacking sequence of each individual specimen would be excessively time-consuming and of limited relevance for the investigation of the impact response. Therefore, the material behavior is treated using a homogenized description at the laminate scale, which is considered more appropriate for the objectives of the present study.

The specimens investigated in this work are directly extracted from seven previously manufactured C/SiC brake disc rings. The presence of the cooling holes on the disks introduces structural discontinuities that are expected to influence the local stress field and impact response. This provides the opportunity to investigate the influence of holes acting as structural discontinuities on the impact response of the material. Due to material availability, six specimens were obtained from each ring segment. Previous investigations on impact testing of ceramic matrix have highlighted that specimen geometry is a critical factor affecting the representativeness of the results. In particular, excessively narrow specimens were found to be strongly affected by edge effects, leading to non-representative stress states under impact loading. For this reason, the present specimens were designed to maximize both longitudinal and transverse in-plane dimensions within the geometric constraints imposed by the available geometry. The average specimen dimensions are reported in Table 1.

Table 1 – Average specimens' dimensions.

Length (mm)	110.25 ± 0.11
Width (mm)	50.11 ± 0.06
Thickness (mm)	8.24 ± 0.15
Holes diameter (mm)	6.06 ± 0.20

Each exhibit a periodic hexagonal hole pattern, which has a 60° rotational symmetry, implying that all six specimens extracted from a single disk share an identical hole configuration. For comparison purposes, a hole-free disc was also provided and used as a reference configuration. An image of a brake disc ring and the specimens extracted from it is shown in Figure 1.

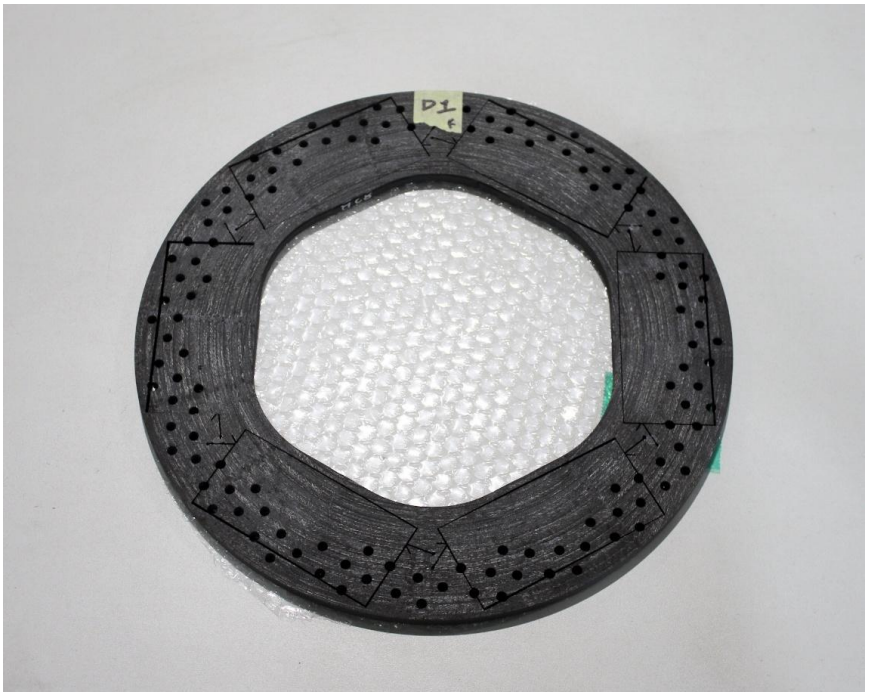


Figure 1 – Complete braking band with the extraction layout of the six specimens.

2.2 Strength test assessment

To define a testing configuration for the evaluation of residual strength, the specific features of ceramic matrix composites were considered. Unlike polymer matrix composites, these materials are characterized by a tensile strength that is typically lower than their compressive strength and are less

prone to delamination under impact loading. As such, three-point bending tests were selected due to their simplicity of execution and effectiveness.

It should however be noted that, when a specimen of non-negligible width is subjected to bending, a secondary anticlastic curvature develops along its width. This curvature can modify the stress distribution within the specimen, particularly in the regions in contact with the machine supports, generating undesired stress concentrations that may potentially lead to specimen failure in these areas. To account for this, two preliminary three-point bending tests were carried out by inserting a 2 mm thick elastomer layer between the specimen and the supports, in order to redistribute possible load concentrations. In addition, a set of strain gauges was applied to the specimen. Two uniaxial strain gauges were installed on the front and rear surfaces to measure transverse strains, and thus the anticlastic curvature. Two biaxial strain gauges were also applied on the front and rear surfaces to detect possible specimen torsion. Both pairs were positioned at mid-distance between one of the supports and the loading cylinder. Along the specimen width, they were placed at mid-width of the unperforated region, i.e., at one quarter of the total width.

The three-point bending configuration used loading cylinders with a diameter of 15 mm and a support span of 90 mm. A photograph of the experimental setup and a schematic of the strain gauge configuration is shown in Figure 2. The tests were conducted under a loading cylinder displacement rate of 0.5 mm/min.

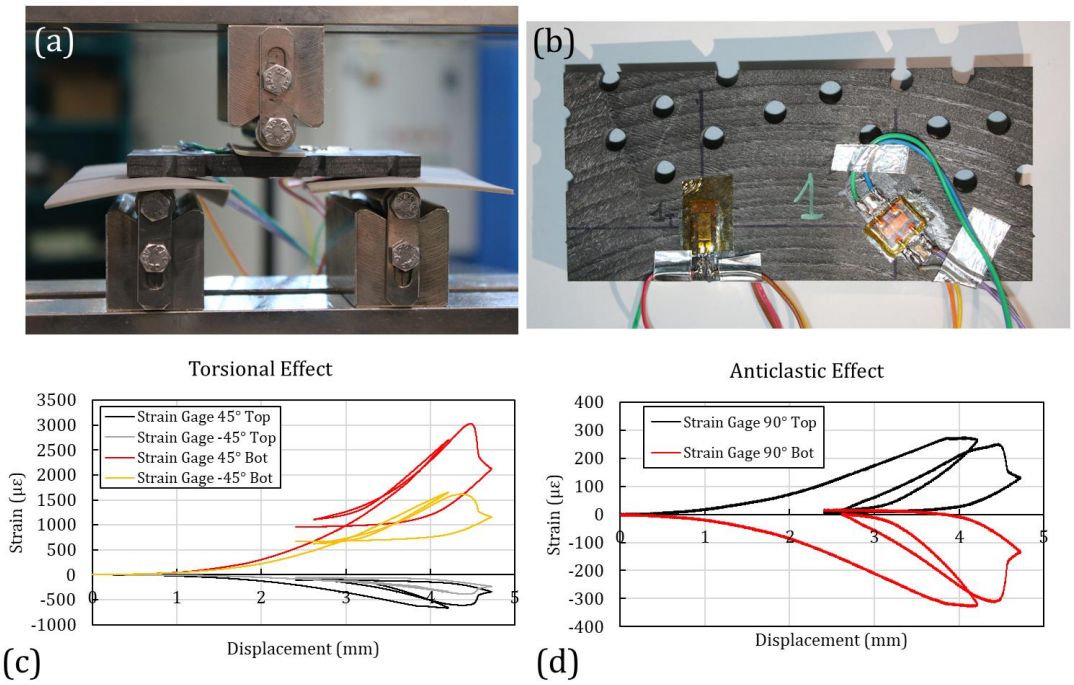


Figure 2 – (a) Three-point bending and (b) strain gages configuration. (c) ±45° strain showing the torsion of the specimen and (d) ±90° strain showing the anticlastic curvature.

Preliminary flexural tests highlighted the presence of secondary deformation modes, including specimen torsion and anticlastic curvature, associated with the geometric configuration. Nevertheless, despite these three-dimensional deformation effects, crack initiation was consistently observed in correspondence with the holes, confirming their dominant role as stress concentration sites governing failure onset.

Load–unload cycles also revealed the progressive accumulation of residual deformation together with a marked asymmetry between tensile and compressive strains, with larger deformation levels systematically measured on the tensile side. This behavior is consistent with the typical nonlinear response of ceramic matrix composites, where matrix cracking, interfacial debonding, frictional sliding, and localized fiber–matrix interactions contribute to irreversible deformation and tension–compression asymmetry.

Based on these preliminary observations, the final testing configuration was modified by removing the silicone pads previously adopted in the fixture.

2.3 Low-energy impact test

Low-energy impact tests were performed using steel impactors accelerated through a guided drop system mounted on a rigid support structure. Two classes of impactors were employed: steel bearing spheres with masses of 28 g and 67 g, respectively, and a cylindrical steel projectile with a hemispherical head and a total mass of 0.533 kg.

The spherical impactors were released through lateral openings positioned at predefined heights along an inclined guide tube, allowing the impact energy to be controlled through the drop height. The inclination of the tube ensured that, after impact, the projectile rebounded away from the specimen, thus preventing multiple impacts on the same location. The heavier projectile was instead lowered to the prescribed height using a nylon wire, which was tensioned immediately after impact in order to suppress secondary rebounds. Since the investigated material exhibits highly dissipative behavior under impact loading, the first impact event is responsible for the majority of the induced damage, while possible secondary contacts provide only a negligible contribution to the overall damage state.

The impact velocity was measured using two photocells positioned near the tube exit and separated by a distance of 100 mm, with an acquisition frequency of 125 kHz. In addition, each test was recorded using a high-speed camera in order to accurately verify the accuracy of the impact location. The specimens were mounted using a fixture derived from the ASTM D7136 standard for impact testing of composite laminates. The fixture, shown in Figure 4, featured a rectangular unsupported window of 100 mm × 75 mm. The specimens, having a total length of 110 mm, were positioned along the short side of the opening, resulting in an effective support length of approximately 17.5 mm on each side. Thin aluminum strips were placed above the specimen in correspondence with the supports and clamped using the fixture fastening system. This configuration ensured adequate specimen restraint while avoiding excessively rigid constraints that could artificially inhibit the flexural deformation induced by impact loading. Several impact tests were performed to investigate the relationship between impact energy, damage detectability, the dominant damage mechanisms, and the residual flexural strength.



Figure 3 – Low energy impact fixture derived from the ASTM D7136 with a detail of the drop tube with the photocells, and of the used impactor.

The damage morphology of the impacted specimens was investigated through visual and tactile inspection, revealing several clear trends. These inspection techniques were selected because of their simplicity and widespread adoption in practical applications. Within a damage-tolerant design framework, damage assessment must account for the detectability limits associated with the specific inspection procedures employed in service.

Below a certain impact energy threshold, no damage could be detected through either visual or tactile inspection. Conversely, above this threshold, hereafter referred to as the detectability threshold or Barely Visible Impact Damage (BVID) threshold, small cracks started to appear on the specimens.

These cracks were consistently observed on the tensile side opposite to the impact location and typically initiated at the hole closest to the specimen edge. The damage propagated over a limited distance along the specimen width, generally remaining confined to a single ply through-thickness. Due to the intrinsic heterogeneity and reflectivity of the impacted surface, these fine cracks are often difficult to detect by visual inspection unless appropriate lighting orientation is used. In this context, tactile inspection proved more effective in identifying and assessing the presence and extent of cracking.

Additional optical microscopy analyses were carried out on the compressed face of selected specimens. In particular, a 20 mm × 20 mm surface region was accurately examined before and after the impact test, again showing no detectable surface degradation. An example of this analysis is reported in Figure 4, where a collage composed of twenty microscope images was assembled to enable a detailed comparison of the investigated area before and after impact. These observations further confirm that the dominant damage mechanisms develop on the tensile side of the specimen, while the impacted surface remains substantially unaffected due to the high local stiffness of the ceramic matrix.

Optical microscopy analyses of the developed cracks indicate a matrix-dominated cracking mechanism, in which fiber–matrix interactions significantly influence crack propagation. In particular, fibers contribute to crack deflection along their preferential orientation, partial crack bridging, and localized fiber pull-out. These mechanisms collectively increase the tortuosity of the crack path and contribute to energy dissipation during damage evolution. Examples of the observed crack morphologies are shown in Figure 4.

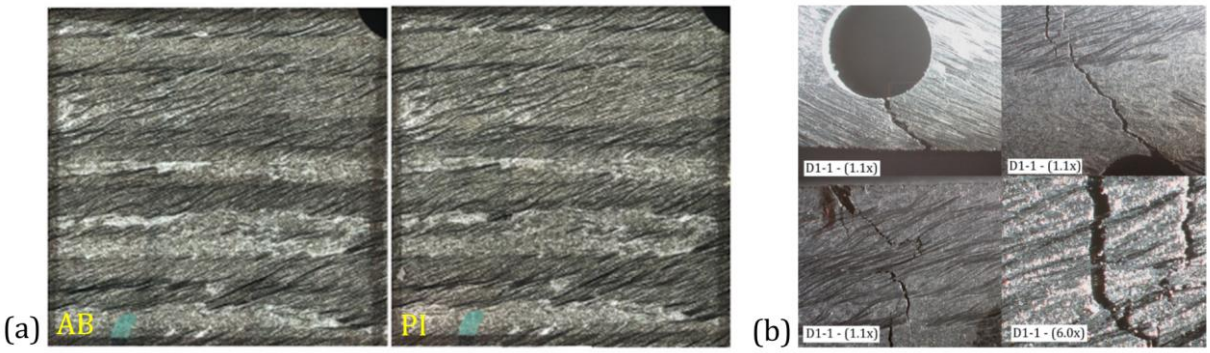


Figure 4 – (a) Impact point on the same specimen: As-Built (AB) vs. Post Impact (PI). (b) Optical microscopy analysis of the typical flexural damage on the tensed side of the specimen.

At impact energies corresponding to approximately 120% of the detectability threshold, a through-width crack was typically observed. The crack generally initiated at the holes located near the specimen edge and propagated across the entire specimen width, resulting in a well-developed fracture path that was more easily detectable. Examples of the crack morphologies associated with 120% of the threshold are reported in Figure 5.

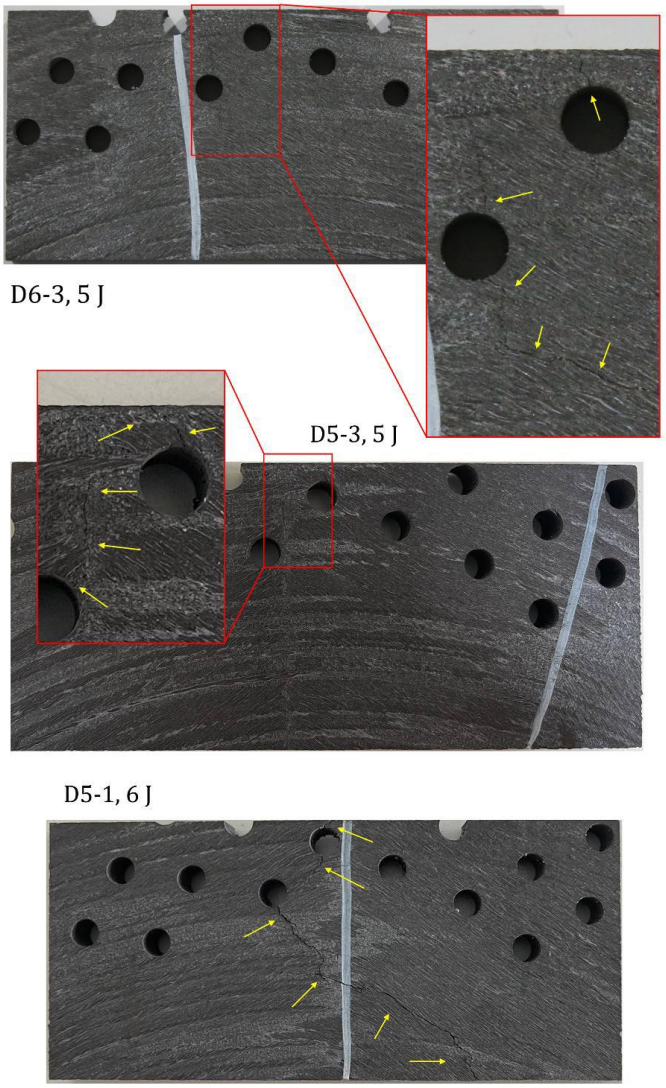


Figure 5 – Typical crack morphology of a specimen impacted with an energy exceeding the BVID threshold.

2.4 Residual strength assessment

Impacted specimens were subsequently subjected to residual flexural strength assessment using the previously described procedure. In Figure 6, the flexural responses of the as-built specimens are reported in black, while those of the impacted specimens are shown in red.

On average, the overall mechanical response remained qualitatively consistent after impact, even if the peak values clearly decreases. An initial linear elastic regime was observed, followed by a smooth transition toward a mildly nonlinear behavior prior to reaching the ultimate stress, here assumed as the flexural strength. This first nonlinear regime can be associated with the pseudo-plastic and frictional mechanisms typically observed in ceramic matrix composites, as also confirmed by the accumulation of limited residual deformation during load–unload cycles. Beyond the peak load, the load-bearing capability decreased progressively rather than catastrophically, evolving toward an extended plateau region. This second nonlinear regime is associated with stable crack propagation through the specimen thickness and highlights the significant fracture toughness of the material. Such behavior is primarily related to crack deflection, crack bridging, and pull-out mechanisms promoted by fiber reinforcement architecture.

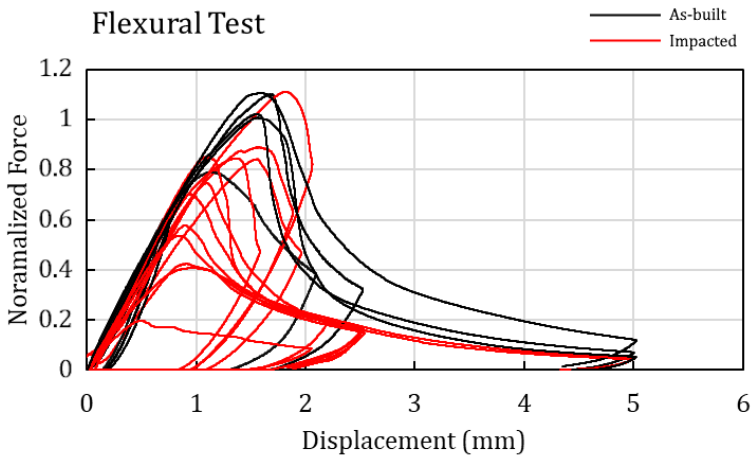


Figure 6 – Force/displacement curves from three-point bending test of as-built and Impacted specimens, showing a common trend with a progressive reduction of the maximum load for the impacted ones.

In Figure 7, the flexural strength, normalized with respect to the average strength of the as-built specimens, is plotted as a function of the impact energy normalized by the detectability, or BVID, threshold. The results reveal a clear trend. Specimens impacted at energy levels below the BVID threshold exhibited negligible reductions in residual flexural performance, whereas impacts corresponding to the BVID threshold already produced an average strength reduction of approximately 38–40%. For impact energies exceeding the BVID threshold, the residual strength decreased dramatically, with reductions exceeding 60% compared to the as-built configuration.

This transition corresponds to the onset of detectable cracking, indicating that the BVID threshold represents a critical condition at which the induced damage becomes structurally significant despite remaining difficult to identify through conventional inspection techniques. These observations further support the necessity of adopting a damage-tolerant design approach for this class of materials and structures.

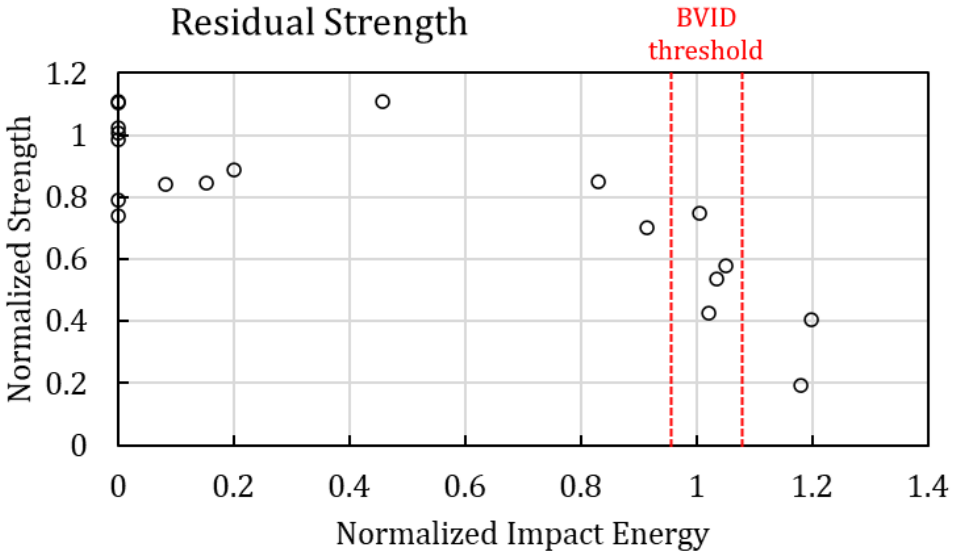


Figure 7 – Flexural strength as a function of impact energy, showing the progressive reduction in strength with increasing impact energy. It is noteworthy that a significant strength reduction is already observed within the BVID region.

2.5 Fatigue test

Fatigue tests were conducted to investigate crack growth and stiffness degradation under cyclic loading. Specimens were tested under three-point bending for up to one million cycles at a frequency of 15 Hz. Both as-built specimens and specimens impacted at the BVID energy threshold were tested

at 50%, 75%, and 90% of their respective reference static strengths. To monitor possible damage evolution, the fatigue tests were periodically interrupted for visual inspection of the specimens and evaluation of crack propagation. Initially, inspections were performed every 100,000 cycles, while at later stages the interruption interval was increased to 200,000 cycles. This procedure allowed the direct assessment of the stability of pre-existing cracks throughout the fatigue campaign. An example of the results of the visual inspection during the fatigue testing is shown in Figure 8, in which no evident evolution or propagation of the crack was observed. Moreover, these photos are a good example of the visual detectability of a BVID.

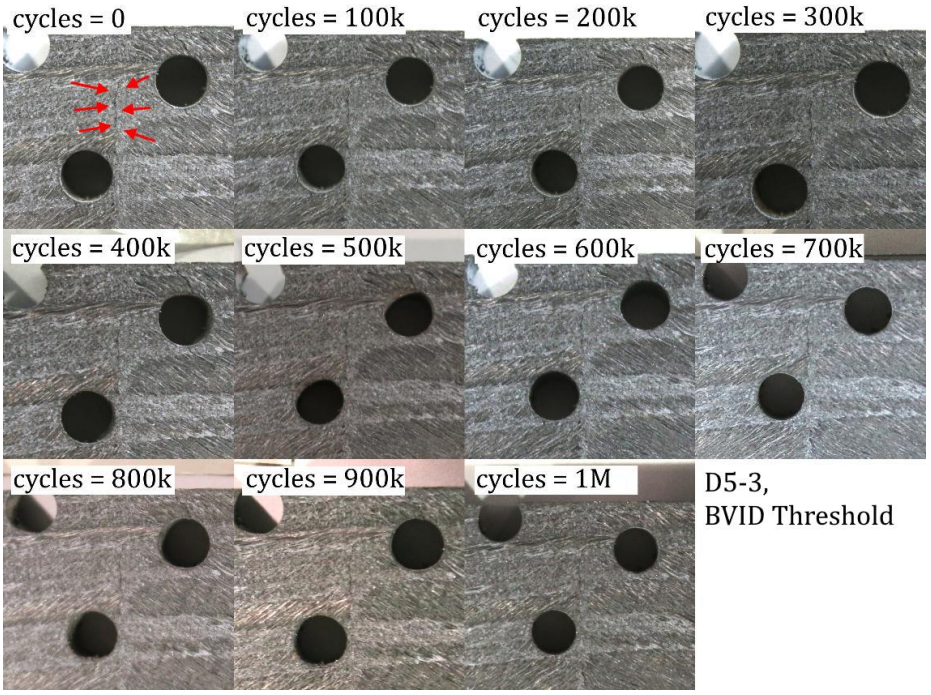


Figure 8 – Visual inspection of BVID during the fatigue testing every 100k cycles.

The results consistently demonstrated the absence of crack propagation, stiffness degradation, or catastrophic failure for load levels up to 75% of the static strength, regardless of the presence of impact damage. Stiffness evolution curves generally exhibited a slight initial increase, attributed to internal settling phenomena rather than damage accumulation. Minor variations observed between measurement intervals were associated with repositioning effects caused by the periodic removal and reinstallation of the specimens for inspection purposes. An example of the stiffness evolution as a function of the number of fatigue cycles for both an as-built specimen and a BVID-impacted specimen is reported in Figure 9. On the other hand, specimens containing a pre-existing, fully developed through-width crack typically failed within a few cycles, exhibiting a quasi-static fracture behavior rather than a fatigue-driven failure mechanism. Overall, the fatigue campaign confirms the excellent fatigue tolerance of C/SiC, even in the presence of BVID-level defects. Provided that operational loads remain below approximately 75% of the static strength, the material exhibits no evidence of cumulative damage growth, making it well suited for applications involving repeated flexural loading and occasional low-energy impacts.

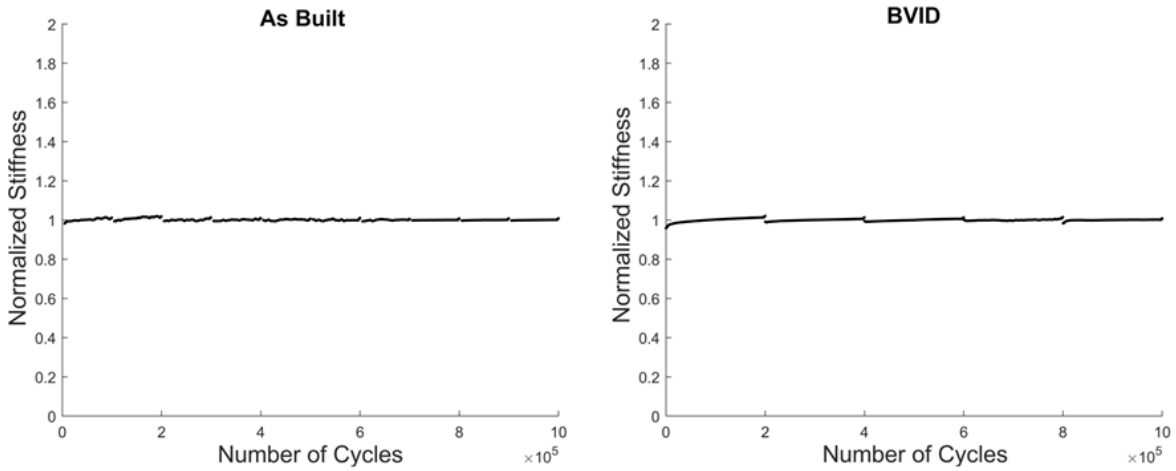


Figure 9 – Flexural stiffness evolution as a function of cycles during the fatigue tests.

3. Numerical modelling

The objective of the present numerical activity was not the detailed reproduction of the underlying physical damage mechanisms, but rather the extraction of additional information from the experimental campaign and the development of engineering-oriented design tools. The final objective was the identification of constitutive laws and material properties suitable for structural design applications, accounting for the degradation induced by different impact energy levels. Consequently, the numerical activity was focused on modeling the residual flexural behavior of the specimens, using the experimentally observed impact damage as an input condition for the constitutive response.

As previously discussed, due to the intrinsic heterogeneity of the material and the manufacturing process, reconstructing the exact stacking sequence of each individual specimen would provide limited benefit. Moreover, from a design perspective, it would not be meaningful to analyze impact events occurring at a specific local arrangement of plies or constituents. Instead, the objective is to identify an average, representative structural response that can be effectively employed within a design framework.

For these reasons, a homogenized modeling approach was adopted. The material was therefore treated as an equivalent continuum with effective mechanical properties representative of the global structural response, rather than explicitly modeling the individual plies and mesoscopic constituents.

3.1 Model definition

The finite element models were developed using SIMULIA Abaqus. The geometry of each specimen was reproduced according to the corresponding extracted component region, accounting for the fact that specimens obtained from the same disc shared the same hole pattern.

The resulting geometries were discretized using C3D8R reduced-integration hexahedral elements with an average characteristic size of approximately 1 mm. The final meshes consisted of roughly 60,000 nodes and 50,000 elements for each specimen configuration. A representative example of the adopted geometry and finite element mesh is reported in Figure 10.

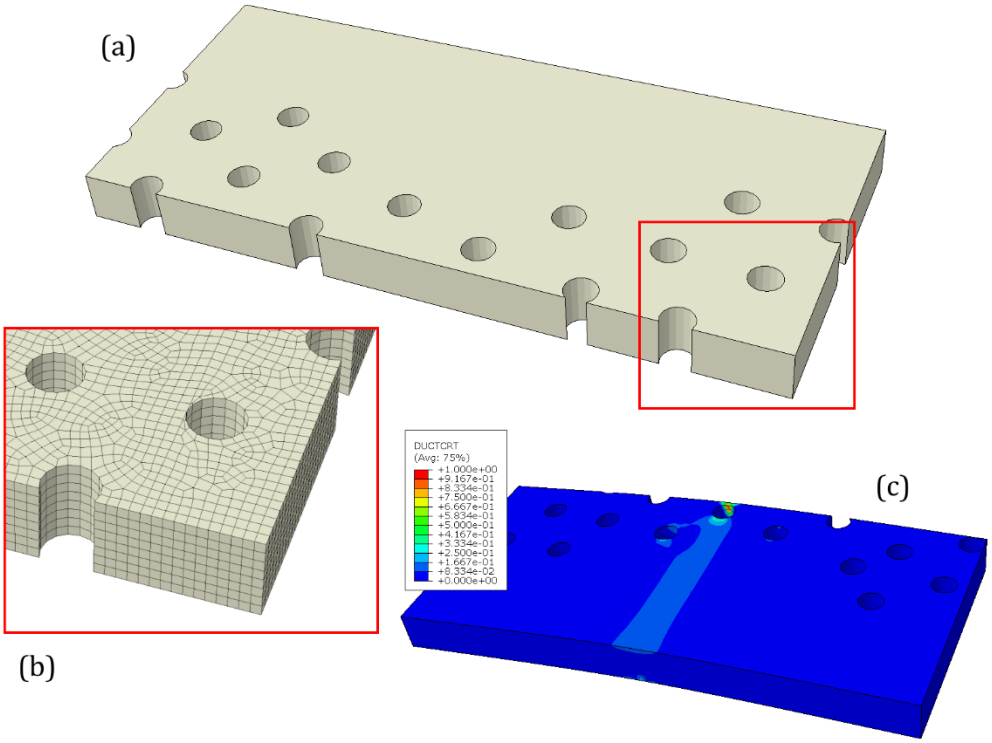


Figure 10 – (a) Reconstructed CAD specimen geometry, (b) detail of the mesh, and (c) contour of the scalar quantity indicating the distance of the current stress state from the ductile criterion.

The flexural test of each specimen was simulated using an elastoplastic constitutive model based on the von Mises yield criterion. Within this framework, the material was assumed to exhibit isotropic behavior together with symmetric tensile and compressive responses. Although C/SiC materials typically exhibits anisotropy and a certain tension–compression asymmetry, these assumptions were considered in line with the homogenized modeling approach adopted in the present work. The influence of Poisson's ratio on the global structural response was found to be limited; therefore, a reasonable constant value of 0.2 was adopted for all simulations. The boundary conditions reproduced the experimental three-point bending configuration. Vertical displacements were constrained at the nodes corresponding to the support locations of the testing fixture, while the applied load was simulated through an imposed displacement prescribed to the nodes corresponding to the loading cylinder. The structural response was then evaluated by monitoring the resulting reaction force. The elastic and plastic parts of the constitutive law were calibrated for each specimen in order to reproduce the corresponding experimental force–displacement curve. In addition, the failure strain parameter was tuned so that the ductile failure criterion, which uses an equivalent plastic strain threshold, reached a value equal to one at the same loading condition corresponding to the experimentally observed specimen failure. The flexural response was therefore simulated only up to the onset of damage, corresponding to the maximum load (ultimate stress) measured experimentally. Beyond this point, no post-peak degradation or fracture propagation was explicitly modeled. Examples of the correlation between numerical and experimental results are reported in Figure 11.

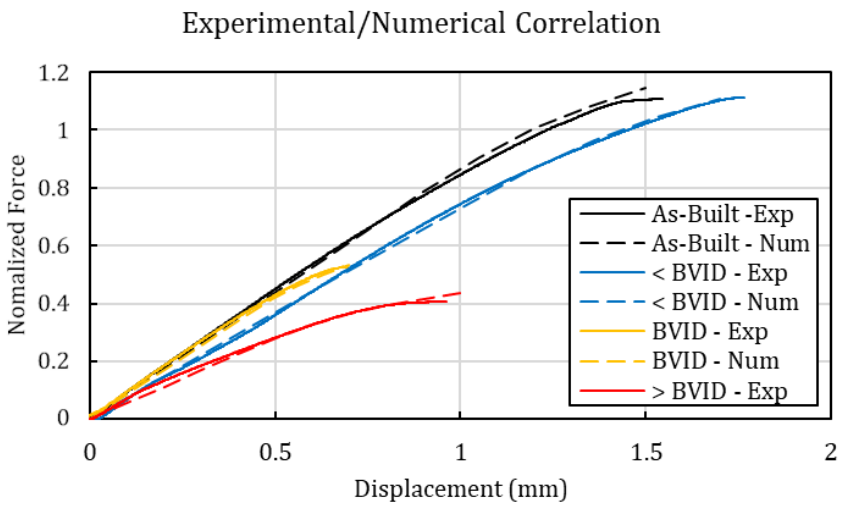


Figure 11 – Correlation between experimental and numerical flexural curves for four specimens impacted at four different impact energy level.

From the calibration of all numerical force/displacement curves against the corresponding experimental flexural responses, a set of effective elastoplastic constitutive laws was obtained. In particular, a specific material law was identified for each specimen, accounting for its individual geometric features and damage state induced by the prior impact loading history. This procedure resulted in a distribution of calibrated constitutive responses rather than a single material model. This approach allowed the identification of distributions for the main material parameters, including Young's modulus, yielding stress, failure stress, and plastic strain at failure, as a function of the impact energy. Here, the yielding stress was identified as the stress level corresponding to the first appreciable deviation from the initial linear elastic response of the force/displacement curve.

In Figure 12, these distributions are reported in terms of average value and standard deviation, distinguishing between as-built specimens and specimens impacted below, around, and above the BVID threshold. The obtained results show that, for impact energies below the BVID threshold, the failure stress remained substantially unaltered, while Young's modulus and yielding stress exhibited reductions not exceeding approximately 15%. Conversely, the plastic strain at failure decreased by nearly 50%. This behavior suggests that, although the material retained most of its elastic load-bearing capability, significant irreversible deformation mechanisms had already developed during impact, effectively consuming a considerable portion of the available plastic reserve.

For impact energies around the BVID threshold, a significant reduction in both yielding stress and ultimate stress was observed, consistently with the onset of the first barely detectable cracks. For impact energies above the BVID threshold, the degradation of the constitutive properties became even more pronounced, confirming the strong influence of impact-induced damage on the residual structural behavior.

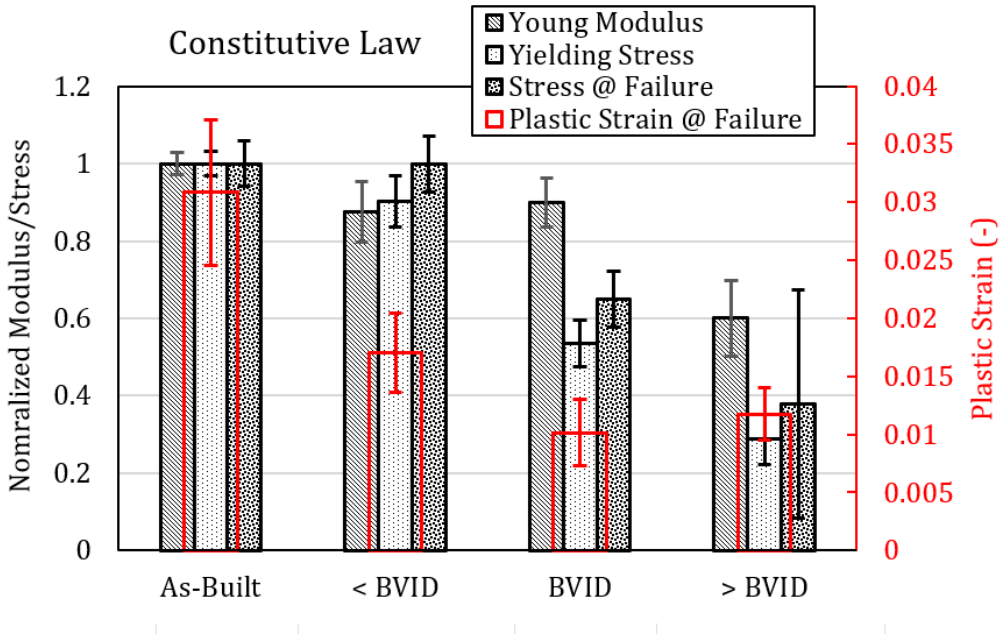


Figure 12 – Distributions of properties of the elastoplastic constitutive law for different impact energy ranges.

Therefore, the material properties identified for specimens impacted at the BVID threshold can be regarded as admissible design properties for an impact-tolerant structural approach. In this context, the constitutive parameters obtained at the BVID condition represent a conservative but still operational material state, corresponding to the presence of structurally significant yet barely detectable damage. Such properties can therefore be adopted as reference values for the design and verification of components required to maintain structural integrity after accidental low-energy impact events.

4. Conclusions

The present investigation provided an integrated experimental and numerical characterization of the impact-damaged flexural behavior of drilled C/SiC composites reinforced with a three-dimensional continuous carbon fiber architecture. The study demonstrated that the material exhibits high impact tolerance and remarkable residual fatigue performance, while also highlighting the critical role of geometrical discontinuities such as holes in governing damage initiation.

Low-energy impact tests allowed the identification of a detectability threshold, or BVID, associated with the onset of small tension-induced cracks originating from the holes closest to the specimen edges. Although such damage remained difficult to identify through conventional visual inspection techniques, its influence on the residual structural response was shown to be significant. In particular, impact energies around the BVID threshold already produced substantial reductions in residual flexural strength, while higher energies resulted in severe degradation of the constitutive properties and structural load-bearing capability.

Despite this reduction in static strength, the fatigue campaign demonstrated an excellent tolerance to cyclic loading. No evidence of crack propagation, stiffness degradation, or fatigue-driven failure was observed for load levels up to approximately 75% of the residual static strength, even in the presence of BVID-level defects. These results indicate that the material retains stable damage conditions under repeated loading and confirm the suitability of C/SiC for applications involving combined impact exposure and cyclic service conditions.

From a numerical standpoint, the adopted homogenized modeling strategy proved effective in reproducing the global flexural response of the specimens and in extracting representative constitutive laws associated with different impact damage states. Rather than reproducing the detailed local failure mechanisms, the proposed approach enabled the derivation of engineering-oriented material properties suitable for structural design applications. In particular, the constitutive laws identified at the BVID threshold can be regarded as admissible properties for impact-tolerant structural design, representing a conservative but operational material condition associated with barely detectable yet structurally significant damage.

Overall, the combined experimental and numerical results provide a consistent framework for the structural qualification of C/SiC components subjected to accidental low-energy impacts. The work establishes a direct relationship between impact energy, damage detectability, constitutive degradation, residual strength, and fatigue performance, thereby contributing to the development of reliable damage-tolerant methodologies for advanced ceramic matrix composite structures.

5. Contact Author Email Address

antoniomaria.caporale@polimi.it

6. Copyright Statement

The authors confirm that they, and/or their company or organization, hold copyright on all of the original material included in this paper. The authors also confirm that they have obtained permission, from the copyright holder of any third party material included in this paper, to publish it as part of their paper. The authors confirm that they give permission, or have obtained permission from the copyright holder of this paper, for the publication and distribution of this paper as part of the ICAS proceedings or as individual off-prints from the proceedings.

7. DOI Number

https://doi.org/10.71945/icas2026_0357

References

[1] N. P. Bansal and J. Lamon, Eds., *Ceramic Matrix Composites: Materials, Modeling and Technology*, 1st ed. Wiley, 2014. doi: 10.1002/9781118832998.

[2] W. Krenkel, “C/C-Sic Composites for Hot Structures and Advanced Friction Systems,” in *Ceramic Engineering and Science Proceedings*, vol. 24, W. M. Kriven and H.-T. Lin, Eds., Hoboken, NJ, USA: John Wiley & Sons, Inc., 2003, pp. 583–592. doi: 10.1002/9780470294826.ch85.

[3] W. Krenkel, “Carbon Fiber Reinforced CMC for High-Performance Structures,” *Int J Applied Ceramic Tech*, vol. 1, no. 2, pp. 188–200, Apr. 2004, doi: 10.1111/j.1744-7402.2004.tb00169.x.

[4] R. Kochendörfer and N. Lützenburger, “Applications of CMCs Made via the Liquid Silicon Infiltration (LSI) Technique,” in *High Temperature Ceramic Matrix Composites*, 1st ed., W. Krenkel, R. Naslain, and H. Schneider, Eds., Wiley, 2001, pp. 275–287. doi: 10.1002/3527605622.ch45.

[5] W. Krenkel and F. Berndt, “C/C–SiC composites for space applications and advanced friction systems,” *Materials Science and Engineering: A*, vol. 412, no. 1–2, pp. 177–181, Dec. 2005, doi: 10.1016/j.msea.2005.08.204.

[6] W. Krenkel and P. Schanz, “Fiber ceramic structures based on liquid impregnation technique,” *Acta Astronautica*, vol. 28, pp. 159–169, Aug. 1992, doi: 10.1016/0094-5765(92)90021-A.

[7] A. M. Caporale, P. Galizia, B. Zanardi, A. Vinci, D. Sciti, and A. Airoldi, “A bi-phasic numerical approach for non-linear response and stiffness recovery related to residual thermal stress in UHTCMCs,” *Journal of the European Ceramic Society*, p. S0955221924002565, Mar. 2024, doi: 10.1016/j.jeurceramsoc.2024.03.038.

[8] D. Jiang, H. Qian, Y. Xu, D. Zhang, and J. Zheng, “Residual strength of C/SiC composite after low-velocity impact,” *Materials Today Communications*, vol. 30, p. 103140, Mar. 2022, doi: 10.1016/j.mtcomm.2022.103140.

[9] H. Mei, C. Yu, Y. Xu, D. Han, and L. Cheng, “Effect of impact energy on damage resistance and mechanical property of C/SiC composites under low velocity impact,” *Materials Science and Engineering: A*, vol. 687, pp. 141–147, Feb. 2017, doi: 10.1016/j.msea.2017.01.062.

[10] Y. Lin and B. Liu, “Study on Impact Resistance of C/SiC Ceramic Matrix Composites for Thermal Protection of the Aerospace Vehicle,” *Mathematical Problems in Engineering*, vol. 2021, pp. 1–10, Aug. 2021, doi: 10.1155/2021/6255014.

[11] G. Janszen, A. M. Caporale, L. Cavalli, M. D. S. Fumo, and A. Airoldi, “Impact tolerance of ceramic matrix composites for aerospace applications,” presented at the ICAS 2024, Florence, Italy.

[12] “AC 23-13A - Fatigue, fail-safe and damage-tolerance evaluation of metallic structure for normal, utility, acrobatic and commuter category airplanes,” Federal Aviation Administration, 2005.